

See discussions, stats, and author profiles for this publication at: <https://www.researchgate.net/publication/279862187>

Effect of epitaxial strain on tunneling electroresistance in ferroelectric tunnel junctions

Article *in* Nanotechnology · July 2015

DOI: 10.1088/0957-4484/26/30/305202 · Source: PubMed

CITATIONS

3

READS

139

6 authors, including:



H. W. Lu

Lanzhou Jiaotong University

181 PUBLICATIONS 2,889 CITATIONS

[SEE PROFILE](#)



Shijie Li

University of Nebraska at Lincoln

4 PUBLICATIONS 20 CITATIONS

[SEE PROFILE](#)



Evgeny Tsymbal

University of Nebraska at Lincoln

320 PUBLICATIONS 8,517 CITATIONS

[SEE PROFILE](#)



Alexei Gruverman

University of Nebraska at Lincoln

236 PUBLICATIONS 7,495 CITATIONS

[SEE PROFILE](#)

Some of the authors of this publication are also working on these related projects:



field control of magnetism [View project](#)



Emergent properties at oxides interfaces [View project](#)

All content following this page was uploaded by [Alexei Gruverman](#) on 17 July 2015.

The user has requested enhancement of the downloaded file. All in-text references underlined in blue are added to the original document and are linked to publications on ResearchGate, letting you access and read them immediately.

Effect of epitaxial strain on tunneling electroresistance in ferroelectric tunnel junctions

This content has been downloaded from IOPscience. Please scroll down to see the full text.

[View the table of contents for this issue](#), or go to the [journal homepage](#) for more

Download details:

IP Address: 129.93.32.103

This content was downloaded on 16/07/2015 at 14:46

Please note that [terms and conditions apply](#).

Effect of epitaxial strain on tunneling electroresistance in ferroelectric tunnel junctions

A Sokolov, O Bak, H Lu, S Li, E Y Tsymbal and A Gruverman

Department of Physics and Astronomy & Nebraska Center for Materials and Nanoscience, University of Nebraska, Lincoln, NE 68588, USA

E-mail: sokolov@unl.edu

Received 17 February 2015, revised 26 May 2015

Accepted for publication 8 June 2015

Published 7 July 2015



Abstract

We report the effect of compressive strain on the tunneling electroresistance (TER) effect in BaTiO₃/SrRuO₃ (BTO/SRO) heterostructures. We find that epitaxial strain imposed by the mismatch of NdGaO₃ and SrTiO₃ lattice parameters with the BTO and SRO layers improves ferroelectric polarization of BTO and concurrently promotes the metallicity of the SRO films. While the enhanced polarization is beneficial for the TER magnitude, the reduced asymmetry in the tunneling barrier due to the shortened screening length of SRO is detrimental for the effect. Thus, a combined effect of strain on the polarization of the ferroelectric barrier and the screening properties of the electrodes needs to be taken into account when considering and predicting the TER effect in ferroelectric tunnel junctions.

Keywords: tunneling electroresistance, ferroelectric thin films, switching effect, epitaxial oxides thin film

(Some figures may appear in colour only in the online journal)

1. Introduction

Ferroelectric tunnel junctions (FTJs) have recently aroused significant interest due to their fascinating properties useful for applications in nanoelectronics, spintronics and data storage [1–3]. A typical FTJ consists of two metal electrodes separated by a nanometer-thick ferroelectric barrier layer, which allows electron tunneling through it. The key property of the FTJ is tunneling electroresistance (TER)—a change in the FTJ's electrical resistance upon reversal of ferroelectric polarization [4, 5]. Contrary to the ferroelectric capacitors where leakage currents are detrimental to the device performance, the conductance of a FTJ is the functional characteristic of the device [6]. Based on simple models it was predicted that the TER effect could be as large as several orders of magnitude due to the change in the tunneling potential barrier [4, 5, 7]. These results were elaborated using first-principles calculations of the transport properties of FTJs, which emphasized the importance of the interface bonding as well as evanescent states in TER [8, 9]. Following these

theoretical predictions, three experimental groups have independently measured the TER effect associated with the ferroelectric polarization switching in BaTiO₃ (BTO) [10, 11] and Pb_{1-x}Zr_xTiO₃ [12] ferroelectric films, revealing resistance changes by two–three orders of magnitude. Further progress has been achieved by successful demonstrations of the TER effect in trilayer patterned junctions suitable for device applications [13–18]. These experimental results provided a proof of concept for the FTJ and demonstrated the possibility for thin-film ferroelectrics to be used as a nanoscale barrier in the devices that can store binary information. It was also proposed that the functionality of FTJs could be extended by exploiting ferromagnetic electrodes to create the so-called multiferroic tunnel junctions (MFTJs) [19]. An MFTJ constitutes a four-state resistance device where the resistance is controlled by both, the ferroelectric polarization direction of the barrier and the magnetization alignment of the ferromagnetic electrodes. MFTJs are interesting from the point of view of their multifunctional properties, as has been demonstrated in a number of recent experimental studies [20–23].

The key parameters controlling the TER ratio in FTJs are the polarization of the ferroelectric barrier layer and the screening length in the adjacent electrodes. It is imperative to realize a ferroelectric barrier with a large and stable remnant polarization for both polarization states. It is also important to achieve sufficient asymmetry in the screening lengths of the two metallic electrodes, which largely controls the magnitude of the TER ratio [4]. Note, however, that too large screening length may be detrimental for polarization stability. Optimal parameters controlling FTJ properties may be obtained by varying ferroelectric and electrode materials [24], by interface engineering [25], or/and by the epitaxial strain control [26]. Theoretical [27] and experimental [28] works show growth of compressively strained ferroelectric films enhancing the polarization magnitude and aligning it normal to the interface. On the other hand, strain imposed on the entire FTJ during epitaxial growth may also change electronic and transport properties of the electrode materials. This effect is expected to be especially notable for FTJs based on SrRuO_3 (SRO) electrodes due to the strong sensitivity of the SRO thin film properties to epitaxial strain [29]. Such an effect may enhance or reduce the TER, depending on changes in the electronic properties of the interface, which control polarization charge screening and hence the tunneling barrier height. Thus, to achieve the optimum performance of FTJs one needs to consider the strain effect imposed on the electrode material.

In this paper, we report the competing effects of epitaxial strain on the TER effect associated with ferroelectric polarization switching of BTO thin films deposited on SRO electrodes. Using SRO thin films epitaxially grown on single crystals SrTiO_3 (001) (STO) and NdGaO_3 (110) (NGO) substrates we explore the effect of epitaxial strain on structural and electric transport properties of SRO as well as ferroelectric properties of BTO and correlate these properties with the TER measured in the BTO/SRO tunnel junctions. Although the epitaxial strain enhances and stabilizes ferroelectric polarization of BTO, it also improves metallicity of SRO, which leads to the reduction of TER due reduced asymmetry in the screening lengths of the two metal electrodes.

2. Experiment

To address a high sensitivity of the SRO initial growth stage to chemical composition of the surface, prior to deposition the pre-cleaned substrates were chemically etched using NH_4F buffered HF (BHF) solution or modified BHF solution for STO and NGO respectively. Subsequent annealing in O_2 atmosphere resulted in atomically flat substrate with B-site surface termination in accordance with previously described STO [30, 31] and NGO [32] substrates treatment. Deposition was carried out using a multi-target pulsed laser deposition system equipped with a KrF excimer laser ($\lambda=248\text{ nm}$). The SRO layers were grown at 750°C under oxygen pressure of $\sim 125\text{ mTorr}$ using the laser energy density of $\sim 2.2\text{ J cm}^{-2}$ and pulse repetition frequency of 2 Hz. During the subsequent BTO synthesis the temperature and oxygen pressure were

lowered to 700°C and 5 mTorr, respectively. The films were cooled down to room temperature at the rate of 5° min^{-1} under 300 Torr of oxygen pressure. The high-pressure reflection high-energy electron diffraction (RHEED) system was employed for *in situ* monitoring of the heterostructure film growth. The thickness of the BTO films was controlled by monitoring the intensity oscillations of RHEED specular reflection. The crystal structure and thickness of the samples prepared for the SRO properties testing were analyzed using x-ray diffraction (XRD) and x-ray reflectivity techniques (Rigaku SmartLab). During BTO/SRO heterostructure synthesis, the SRO thickness was maintained constant at 17 nm by controlling the number of calibrated laser shots. We continuously employed *in situ* RHEED pattern analysis for initial screening of the samples. Only those exhibiting identical with the substrates RHEED patterns, were used for further analysis. In-plane conductivity of SRO films were tested using standard 4-probe technique using Oxford cryostat system. A commercial atomic force microscopy (AFM) system (MFP-3D, Asylum Research) was used for piezoresponse force microscopy (PFM) testing of polarization state in the BTO layers. Conductive cantilevers probes serve as charge screening top electrode and were employed for polarization imaging and measurement of the *I-V* characteristics of the obtained heterostructures employing a conducting AFM (C-AFM) mode.

3. Results and discussion

3.1. Effect of epitaxial strain on SRO thin film

A number of research groups have reported successful epitaxial growth of the SRO films up to several tens of nanometers on the STO (001) substrates [33–36]. Growing SRO films on NGO (110) substrates is more challenging [37]. While SRO films grown epitaxially on STO are under 0.6% compressive strain, the films grown of NGO are exposed to 1.7% compressive strain. As the film thickness increases, the large lattice mismatch between NGO and SRO results in structural relaxation. In order to make accurate comparison between epitaxially strained SRO films grown on STO and NGO substrates, one needs to ensure the absence of relaxation. For this purpose, we have prepared and performed x-ray studies of SRO thin films of different thicknesses grown on NGO substrates. Figure 1(a) demonstrates RHEED intensity of specular point during deposition and pattern taken on the 22 nm thick SRO film grown on NGO and STO substrates. The spot intensity oscillated twice and then reached a steady state until the growth was stopped. This behavior of the RHEED intensity represents the fact that the growth mode of the SRO film has a transition from the two-dimensional layer-by-layer to the step-flow mode, widely observed for the SRO films grown on the STO substrates [38]. Positions of RHEED bright spots before and after SRO deposition are shown in figure 1(b). This pattern matches exactly those of the bare substrates and peaks have very small streaking, suggesting atomically smooth film surface with crystallinity similar to the

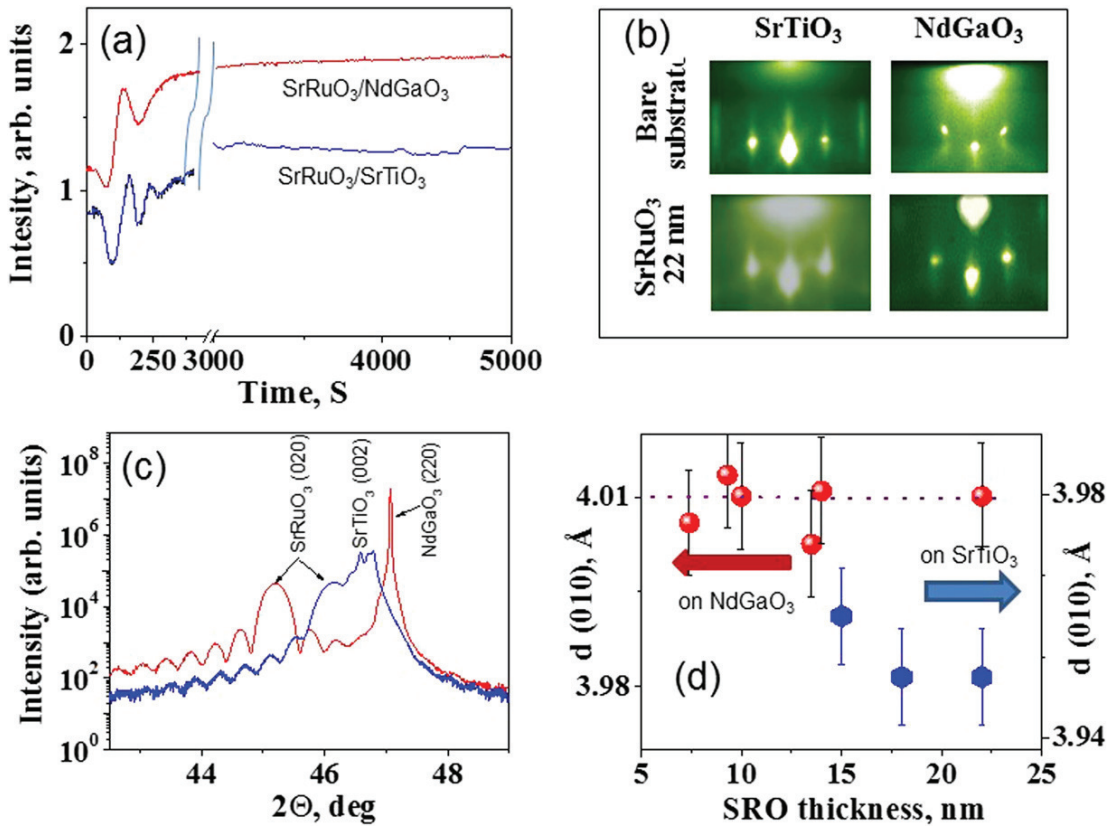


Figure 1. (a) RHEED specular spot intensity during SrRuO₃ deposition on (110) NdGaO₃ substrate. (b) RHEED diffraction pattern before and after 22 nm deposition of SRO on STO (left) and NGO (right). (c) X-ray 2theta-theta profiles of 22 nm thick SrRuO₃ films grown on STO (red) and NGO (blue) substrates. (d) Thickness dependence of the out-of-plane lattice spacing of the SrRuO₃ films grown on the NdGaO₃ and SrTiO₃ substrates.

substrate. The Bragg–Bretano XRD pattern displays only reflections arising from the film and the substrate, and there are no traces of secondary impurity phases. The diffraction peak positions also confirm the (010) out-of-plane orientation of SRO film. Figure 1(c) shows the x-ray 2theta-theta profiles of the 22 nm thick SRO film synthesized on STO and NGO substrates.

The Laue oscillations, whose period corresponds to the film thickness, again indicating very uniform and smooth films. The measured out-of-plane lattice constants of the SRO film are larger than the bulk lattice parameters in both cases (4.01 and 3.95 Å for SRO/NGO and SRO/STO, respectively, as compared to 3.93 Å for bulk SRO). These constants remain unchanged for the entire film thicknesses (in the range up to 22 nm) for the same substrate (figure 1(d)).

To compare the intrinsic properties of SRO thin films grown on the two substrates, which are relevant to the TER effect, we studied the electronic transport properties of the SRO films. To exclude the possibility of relaxation in the outmost SRO layers, a 17 nm thick SRO film was chosen for fabrication and further analysis. Figure 2 shows a temperature dependence of the resistivity $\rho(T)$ of the SRO film on the STO and NGO substrates. Both films clearly demonstrate metallic behavior with a kink at the Curie temperature corresponding

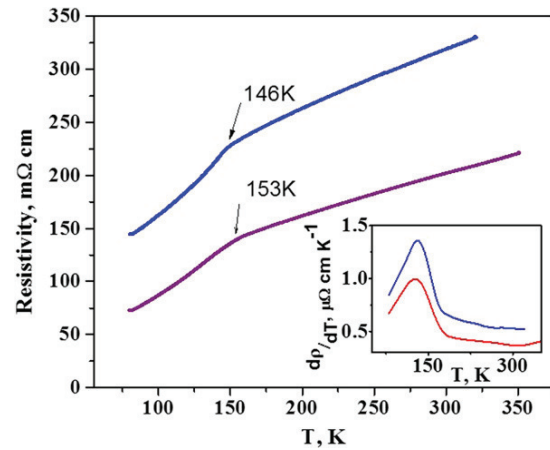


Figure 2. Temperature dependence of the in-plane electrical resistivity ($\rho(T)$) of SrRuO₃/NdGaO₃ (the red curve) and SrRuO₃/SrTiO₃ (the blue curve). Inset shows the derivative ($d\rho/dT$) revealing a pronounced peak at the transition temperature.

to the phase transition between ferromagnetic and paramagnetic states. Analysis of the $d\rho/dT$ characteristics (inset in figure 2) shows that the transitions occur at $T_C=153$ and 148 K for the SRO films grown on the NGO and STO

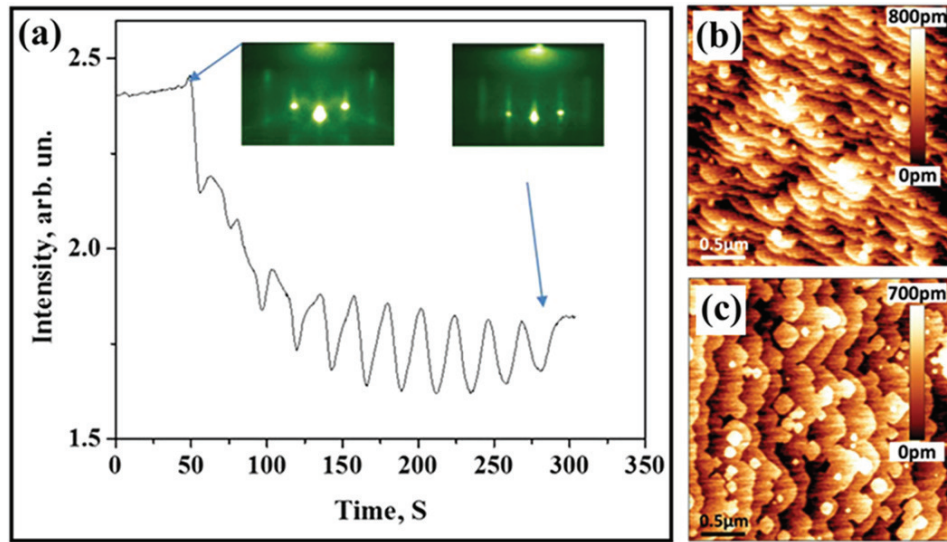


Figure 3. (a) RHEED pattern of BaTiO₃ (11 ML)/SrRuO₃/NdGaO₃ before and after deposition of 11 ML BaTiO₃ thin film. AFM topography of the BaTiO₃(11 ML)/SrRuO₃/NdGaO₃ (b) and BaTiO₃(11 ML)/SrRuO₃/SrTiO₃ (c) films indicating terraces and periodic steps with a unit-cell height.

substrates, respectively. The room temperature resistivity of the SRO/STO sample is about $315 \mu\Omega \text{ cm}$, which is by a factor of 1.6 larger than that of the SRO/NGO sample ($200 \mu\Omega \text{ cm}$). These values are consistent with the results, reported by other groups for SRO films grown on STO [29] and NGO [39] substrates.

This difference in the resistivity may be attributed to the formation of Ru vacancies which are known to strongly affect the resistivity of SRO thin films. It was found that changing the ruthenium stoichiometry in SRO films by varying the oxygen activity during deposition changes the residual resistivity of SRO films [40, 41]. For the stoichiometric samples, the room temperature resistivity was measured to be about $190 \mu\Omega \text{ cm}$, which is similar to what we obtained for SRO films grown on the NGO substrates. When ruthenium vacancies are introduced, this value increases markedly to about $300 \mu\Omega \text{ cm}$ [40] similar to what we measure for SRO/STO samples. Furthermore, the resistivity scales with the volume of the unit cell: according to [40], the resistivity increases by a factor of 1.5 with the volume of the unit cell changing from 240.6 to 241.8 \AA^3 (i.e. by about 0.5%). Our XRD measurements revealed that the volume of the SRO unit cell changed from 240.2 \AA^3 when grown on the NGO substrate to 241.1 \AA^3 on the STO substrate, demonstrating a similar change in the resistivity. We attribute this observations to the presence of Ru vacancies in our films, which is also consistent with decreasing the Curie temperature with increasing Ru vacancy concentration in SRO films [40].

3.2. Effect of epitaxial strain on TER effect in BTO/SRO heterostructure

To elucidate the impact of the epitaxial strain on TER, we have fabricated a set of BTO/SRO/NGO and BTO/SRO/STO

samples and performed PFM and C-AFM studies. The growth of the BTO/SRO heterostructure on STO and NGO substrates was controlled *in situ* by monitoring the RHEED pattern and specular point intensity during the deposition process. Observed intensity oscillations indicate the two-dimensional layer-by-layer growing mode for the BTO film and the peaks intensity represent the formation of a new monolayer (ML), consisting of a full unit cell of BTO perovskite structure (4.05 \AA). Perfect preservation of the initial bright spots pattern and intensity oscillations for 11 ML of BTO film are clearly seen in figure 3(a). The AFM topographic images of the surface morphology in figures 3(b) and (c) show atomically flat terraces with one unit-cell high ($\sim 4 \text{ \AA}$) steps of BTO/SRO heterostructure on both substrates. These results indicate epitaxial structure of the fabricated samples.

To analyze the ferroelectric properties of the fabricated heterostructures, the local switching spectroscopy of 6 ML thick ($\sim 2.4 \text{ nm}$) BTO films has been carried out by means of PFM. The local hysteresis loops shown in figures 4(a) and (c) indicate strong ferroelectric response for both heterostructures. PFM imaging of the electrically poled regions in the BTO films revealed switchable and stable polarization states in the BTO films. Subsequent investigation of the TER effect in the same BTO heterostructures on the SRO/STO and SRO/NGO substrates has been performed by acquiring multiple I - V curves for various locations in the electrically poled regions with polarization pointing up and down (figures 4(b) and (d)). It can be seen that although both films exhibit the resistive switching behavior, the effect is more pronounced in the BTO/SRO/STO samples. The OFF/ON resistance ratio, or TER, was about 20 for the BTO/SRO/STO heterostructure, which agreed well with the previously reported results [11]. However, this ratio was twice as small (about 10) for the BTO/SRO/NGO heterostructure, contrary to the expectation that the larger remnant polarization of BTO due to the larger

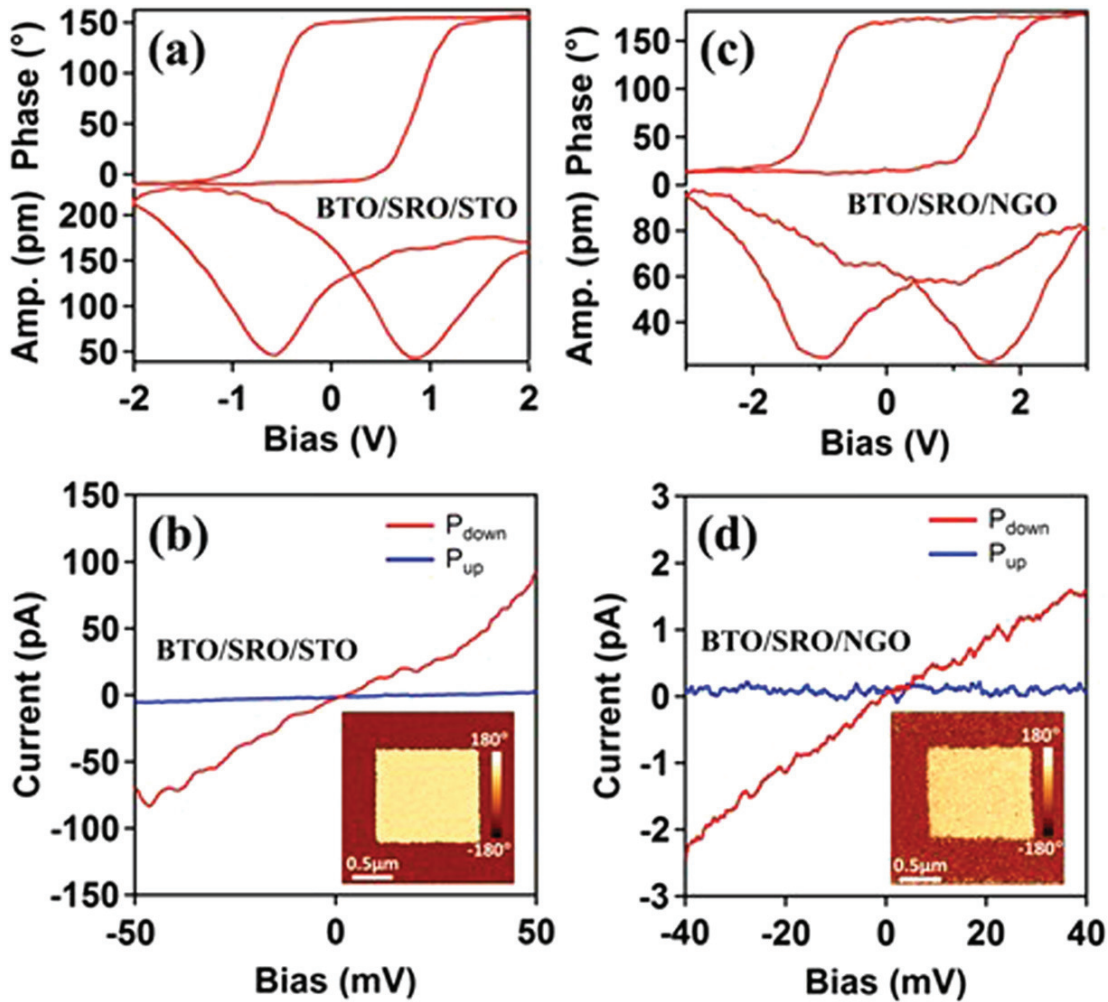


Figure 4. Results of PFM and C-AFM testing of the for 6 ML thick BaTiO₃-based ferroelectric heterostructures grown on SrRuO₃/SrTiO₃ (a), (b) and SrRuO₃/NdGaO₃ (c) and (d). (a) and (c) PFM hysteresis loops and (b), (d) I – V curves obtained in the heterostructures poled downward with +3 V (red curves) and upward with -3 V (blue curves). Insets in (b) and (d) show PFM phase images of the BaTiO₃ films after poling with -3 V (lighter regions) and +3 V (darker regions).

compressive strain induced by the NGO substrate would result in the enhanced TER effect.

We explain this observation in terms of the improved metallicity of the SRO films in the samples grown on the NGO substrates. Changes in the carrier concentration affect the electron screening properties and, thus, alter the tunneling potential barrier seen by the charge carriers. The TER effect magnitude is determined by the asymmetry in the screening lengths of the top (the AFM tip) and bottom (SRO) electrodes. The AFM tip is expected to have excellent screening properties with a screening length typical for a good metal. This layer controls the effective screening length, δ_1 , of the ferroelectric polarization on the BTO film surface. The screening length of the bottom SRO electrode varies under different compressive strains induced by STO and NGO substrates. When grown on the STO substrate, the SRO film has reduced metallic properties manifested in a relatively large screening length (δ_{STO}) at the bottom interface. For the

SRO films grown on the NGO substrate, the larger epitaxial strain improves SRO metallicity and reduces the screening length (δ_{NGO}). This decrease in the SRO screening length under larger strain diminishes the asymmetry of the FTJ heterostructure, hence reducing a change in the average potential barrier height upon polarization reversal which results in the reduced TER effect in the BTO/SRO/NGO heterostructures.

To make these arguments quantitative, we estimate the observed changes in TER under strain. Within a simple Wentzel–Kramers–Brillouin model, the TER ratio can be expressed as follows[11]:

$$\text{TER} = \exp \left[\frac{\sqrt{2m}}{\hbar} \frac{\delta\phi}{\sqrt{\phi}} \right] d, \quad (1)$$

where d is ferroelectric layer thickness, ϕ is the average potential barrier height, and $\delta\phi$ is its change with reversal of

ferroelectric polarization. The latter is given by [4]

$$\delta\phi \approx \frac{edp(\delta_2 - \delta_1)}{\epsilon(\delta_2 + \delta_1)}, \quad (2)$$

where P is ferroelectric polarization and ϵ is background dielectric permittivity [42], δ_1 and δ_2 are screening lengths of the electrodes. For simplicity, we assume that the ferroelectric polarization is uniform across the barrier layer and has the same magnitude P independent of its orientation. In this case we find:

$$\text{TER} \approx \exp \left[\frac{\sqrt{2m}}{\hbar\sqrt{\phi}} \frac{ep(\delta_2 - \delta_1)}{\epsilon(\delta_2 + \delta_1)} d^2 \right]. \quad (3)$$

As is evident from this expression, the TER enhancement resulting from the increased ferroelectric polarization in a more compressively strained film may be outweighed by the decrease in the screening length δ_2 due to the enhanced metallicity of the electrode. (In the limiting case when δ_2 becomes equal to δ_1 the TER effect disappears irrespective of how strongly the polarization is enhanced.) For example, if we assume that ferroelectric polarization is enhanced by a factor of two from $P = 20 \mu\text{C cm}^{-2}$ for the BTO/SRO/STO structure to $P = 40 \mu\text{C cm}^{-2}$ for the BTO/SRO/NGO structure, using typical parameters for BTO-based FTJs ($\epsilon = 100 \epsilon_0$ [43], $m = m_0$, $d = 2.4 \text{ nm}$ and $\delta_1 = 0.5 \text{ nm}$), the experimentally measured values of TER will be observed if the screening length δ_2 will be $\sim 0.9 \text{ nm}$ for the BTO/SRO/STO structure and $\sim 0.7 \text{ nm}$ for BTO/SRO/NGO. The smaller screening length for the SRO electrode on the NGO substrate means that this FTJ is more symmetric; hence, it should have a smaller TER. We see that even though the ferroelectric polarization is expected to be larger for the strained BTO films on the NGO substrate, the smaller difference in the screening lengths between the top and bottom electrodes cancels out the TER enhancement expected for a larger ferroelectric polarization.

4. Conclusion

In conclusion, we have successfully synthesized BTO-based FTJs with different epitaxial strain provided by STO and NGO substrates. Although the ferroelectric polarization of BTO is enhanced when the BTO/SRO heterostructure is grown on the NGO substrate due to a larger compressive strain, the TER effect is reduced. We attribute this phenomenon to the strain-induced changes in the electronic properties of the SRO films. Specifically, we suggest that the reduced TER in BTO/SRO/NGO is due to the enhanced metallicity of SRO, grown on NGO, which reduces asymmetry of the potential profile in this heterostructures. Thus, a combined effect of strain on the ferroelectric polarization of the barrier and the screening properties of the electrodes needs to be taken into account when considering/predicting the TER effect in FTJs.

Acknowledgments

This work was supported by the National Science Foundation (NSF) through the Nebraska Materials Research Science and Engineering Center (MRSEC) under Grant No DMR-1420645 (fabrication of thin films, electrical characterization and modeling) and by the US Department of Energy, Office of Science, Basic Energy Sciences, Division of Materials Sciences and Engineering, under Award DE-SC0004876 (scanning probe measurements). A S acknowledges support from the NSF DMR-1310542 grant (structural characterizations).

References

- [1] Tsymbal E Y and Kohlstedt H 2006 Tunneling across a ferroelectric *Science* **313** 181
- [2] Tsymbal E Y, Gruverman A, Garcia V, Bibes M and Barthélémy A 2012 Ferroelectric and multiferroic tunnel junctions *MRS Bull.* **37** 138
- [3] Garcia V and Bibes M 2014 Ferroelectric tunnel junctions for information storage and processing *Nat. Commun.* **5** 4289
- [4] Zhuravlev M Y, Sabirianov R F, Jaswal S S and Tsymbal E Y 2005 Giant electroresistance in ferroelectric tunnel junctions *Phys. Rev. Lett.* **94** 246802
- [5] Kohlstedt H, Pertsev N A, Rodriguez Contreras J and Waser R 2005 Theoretical current-voltage characteristics of ferroelectric tunnel junctions *Phys. Rev. B* **72** 125341
- [6] Tsymbal E Y and Gruverman A 2013 Ferroelectric tunnel junctions: beyond the barrier *Nat. Mater.* **12** 602
- [7] Zhuravlev M Y, Maekawa S and Tsymbal E Y 2010 Effect of spin-dependent screening on tunneling electroresistance and tunneling magnetoresistance in multiferroic tunnel junctions *Phys. Rev. B* **81** 104419
- [8] Velev J P, Duan C-G, Belashchenko K D, Jaswal S S and Tsymbal E Y 2007 Effect of ferroelectricity on electron transport in Pt/BaTiO₃/Pt ferroelectric tunnel junctions *Phys. Rev. Lett.* **98** 137201
- [9] Velev J P, Duan C-G, Burton J D, Smogunov A, Nirajan M K, Tosatti E, Jaswal S S and Tsymbal E Y 2009 Magnetic tunnel junctions with ferroelectric barriers: prediction of four resistance states from first principles *Nano Lett.* **9** 427
- [10] Garcia V, Fusil S, Bouzehouane K, Enouz-Vedrenne S, Mathur N D, Barthélémy A and Bibes M 2009 Giant tunnel electroresistance for non-destructive readout of ferroelectric states *Nature* **460** 81
- [11] Gruverman A *et al* 2009 Tunneling electroresistance effect in ferroelectric tunnel junctions at the nanoscale *Nano Lett.* **9** 3539
- [12] Maksymovych P, Jesse S, Yu P, Ramesh R, Baddorf A P and Kalinin S V 2009 Polarization control of electron tunneling into ferroelectric surfaces *Science* **324** 1421
- [13] Chanthbouala A *et al* 2012 Solid-state memories using ferroelectric tunnel junctions *Nat. Nanotechnology* **7** 101
- [14] Chanthbouala A *et al* 2012 A ferroelectric memristor *Nat. Mater.* **11** 860
- [15] Kim D J, Lu H, Ryu S, Bark C-W, Eom C-B, Tsymbal E Y and Gruverman A 2012 Ferroelectric tunnel memristor *Nano Lett.* **12** 5697
- [16] Wen Z, Li C, Wu D, Li A and Ming N 2013 Ferroelectric-field-effect-enhanced electroresistance in metal/ferroelectric/semiconductor tunnel junctions *Nat. Mater.* **12** 617
- [17] Lu H, Lipatov A, Ryu S, Kim D J, Lee H, Zhuravlev M Y, Eom C B, Tsymbal E Y, Sinitkii A and Gruverman A 2014

- Ferroelectric tunnel junctions with graphene electrodes *Nat. Commun.* **5** 5518
- [18] Soni R, Petrar A, Meuffels P, Vavra O, Ziegler M, Kim S K, Jeong D S and Pertsev N A Kohlstedt H 2014 Giant electrode effect on tunnelling electroresistance in ferroelectric tunnel junctions *Nat. Commun.* **5** 5414
- [19] Zhuravlev M Y, Jaswal S S, Tsybala E Y and Sabirianov R F 2005 Ferroelectric switch for spin injection *Appl. Phys. Lett.* **87** 222114
- [20] Garcia V V et al 2010 Ferroelectric control of spin polarization *Science* **327** 1106
- [21] Hambe M, Petrar A, Pertsev N A, Munroe P, Nagarajan V and Kohlstedt H 2010 Crossing an interface: ferroelectric control of tunnel currents in magnetic complex oxide heterostructures *Adv. Func. Mater.* **20** 2436
- [22] Pantel D, Goetze S, Hesse D and Alexe M 2012 Reversible electrical switching of spin polarization in multiferroic tunnel junctions *Nat. Mater.* **11** 289
- [23] Yin Y W et al 2013 Enhanced tunnelling electroresistance effect due to a ferroelectrically induced phase transition at a magnetic complex oxide interface *Nat. Mater.* **12** 397
- [24] Barrionuevo D, Zhang L, Ortega N, Sokolov A, Kumar A, Misra P, Scott J F and Katiyar R S 2014 Tunneling electroresistance in multiferroic heterostructures *Nanotechnology* **25** 495203
- [25] Lu H et al 2012 Enhancement of ferroelectric polarization stability by interface engineering *Adv. Mater.* **24** 1209
- [26] Pertsev N A, Zembilgotov A G and Tagantsev A K 1998 Effect of mechanical boundary conditions on phase diagrams of epitaxial ferroelectric thin films *Phys. Rev. Lett.* **80** 1988
- [27] Schlom D G, Chen L-Q, Eom C-B, Rabe K M, Streiffer S K and Triscone J-M 2007 Strain tuning of ferroelectric thin films *Ann. Rev. Mater. Res.* **37** 589
- [28] Choi K J et al 2004 Enhancement of ferroelectricity in strained BaTiO₃ thin films *Science* **306** 1005
- [29] Koster G, Klein L, Siemons W, Rijnders G, Dodge J S, Eom C-B, Blank D H A and Beasley M R 2012 Structure, physical properties, and applications of SrRuO₃ thin films *Rev. Mod. Phys.* **84** 253
- [30] Kawasaki M, Takahashi K, Maeda T, Tsuchiya R, Shinohara M, Ishiyama O, Yonezawa T, Yoshimoto M and Koinuma H 1994 Atomic control of the SrTiO₃ crystal *Science* **266** 1540
- [31] Koster G, Kropman B L, Rijnders G J H M, Blank D H A and Rogalla H 1998 Quasi-ideal strontium titanate crystal surfaces through formation of strontium hydroxide *Appl. Phys. Lett.* **73** 2920
- [32] Leca V, Blank H A and Rijnders G 2012 Termination control of NdGaO₃ crystal surfaces by selective chemical etching *arXiv:1202.2256*
- [33] Eom C B, Cava R J, Fleming R M, Phillips J M, Vandover R B, Marshall J H, Hsu J W P, Krajewski J J and Peck W F 1992 Single-crystal epitaxial thin films of the isotropic metallic oxides Sr_{1-x}Ca_xRuO₃ (0 ≤ x ≤ 1) *Science* **258** 1766
- [34] Ahn C H, Tybella T, Antognazza L, Char K, Hammond R H, Beasley M R, Fischer Ø and Triscone J-M 1997 Local, nonvolatile electronic writing of epitaxial Pb(Zr_{0.52}Ti_{0.48})O₃/SrRuO₃ heterostructures *Science* **276** 1100
- [35] Vailionis A, Siemons W and Koster G 2008 Room temperature epitaxial stabilization of a tetragonal phase in ARuO₃ (A=Ca and Sr) thin films *Appl. Phys. Lett.* **93** 051909
- [36] Grutter A, Wong F, Arenholz E, Liberati M, Vailionis A and Suzuki Y 2010 Enhanced magnetism in epitaxial SrRuO₃ thin films *Appl. Phys. Lett.* **96** 082509
- [37] Kan D, Aso R, Kurata H and Shimakawa Y 2013 Epitaxial strain effect in tetragonal SrRuO₃ thin films *J. Appl. Phys.* **113** 173912
- [38] Choi J, Eom C B, Rijnders G, Rogalla H and Blank D H A 2001 Growth mode transition from layer by layer to step flow during the growth of heteroepitaxial SrRuO₃ on (001) SrTiO₃ *Appl. Phys. Lett.* **79** 1447
- [39] Aso R, Kan D, Fujiyoshi Y, Shimakawa Y and Kurata H 2014 Strong dependence of oxygen octahedral distortions in SrRuO₃ films on types of substrate-induced epitaxial strain *Cryst. Growth Des.* **14** 6478
- [40] Siemons W, Koster G, Vailionis A, Yamamoto H, Blank D H A and Beasley M R 2007 Dependence of the electronic structure of SrRuO₃ and its degree of correlation on cation off-stoichiometry *Phys. Rev. B* **76** 075126
- [41] Dabrowski B, Chmaisssem O, Klamut P W, Kolesnik S, Maxwell M, Mais J, Ito Y, Armstrong B D, Jorgensen J D and Short S 2004 Reduced ferromagnetic transition temperatures in SrRu_{1-x}O₃ perovskites from Ru-site vacancies *Phys. Rev. B* **70** 014423
- [42] Tagantsev A K, Gerra G and Setter N 2008 Short-range and long-range contributions to the size effect in metal-ferroelectric-metal heterostructures *Phys. Rev. B* **77** 174111
- [43] Kim D J, Jo J Y, Kim Y S, Chang Y J, Lee J S, Yoon J-G, Song T K and Noh T W 2005 Polarization relaxation induced by a depolarization field in ultrathin ferroelectric BaTiO₃ capacitors *Phys. Rev. Lett.* **95** 237602